A single amino acid variant in the variable region I of AAV capsid confers liver detargeting

Ruxiao Xing*[1], Mengyao Xu*[1], Darcy Reil[1], April Destefano[1], Mengtian Cui[1], Nan Liu[1], Jialing Liang[1], Guangchao Xu[1], Li Luo[1], Meiyu Xu[1], Fang Zhang[1], Phillip W.L. Tai[1], Alisha M. Gruntman[1], Terence R. Flotte[1], Guangping Gao[#1,2], Dan Wang[#1,3]

[1]Department of Genetic and Cellular Medicine, Horae Gene Therapy Center, University of Massachusetts Chan Medical School, Worcester, MA 01605, USA

[2]Department of Microbiology, University of Massachusetts Chan Medical School, Worcester, MA 01605, USA

[3]RNA Therapeutics Institute, University of Massachusetts Chan Medical School, Worcester, MA 01605, USA

*Co-first authors

[#]Co-corresponding authors

Correspondence should be addressed to:

Dan Wang, Ph.D.
Department of Genetic and Cellular Medicine
UMass Chan Medical School
Worcester, MA 01605, USA
Telephone: +1-(774) 455-4574
Fax: +1-(508) 856-1552
E-mail: Dan.Wang@umassmed.edu

Guangping Gao, Ph.D.
Department of Genetic and Cellular Medicine
UMass Chan Medical School
Worcester, MA 01605, USA
Telephone: +1-(508) 856-3563
Fax: +1-(508) 856-1552
E-mail: Guangping.Gao@umassmed.edu

ABSTRACT

AAV capsid serotypes isolated from nature have been widely used in gene delivery and gene therapy. Recently, more than 1,000 distinct AAV capsids were identified from human clinical samples by high-throughput, long-read DNA sequencing (Hsu HL et al. *Nature Communications* 2020). In this study, we tap into this broad natural biodiversity of AAV capsids to develop liver-tropic AAV capsids. We initially screened a subset of variants derived from AAV8 (n=159) for packaging efficiency. The top 30% of these variants were subjected to a barcoded vector library screen in mice and ferrets for their ability to mediate liver gene transfer. Although no variant surpassed AAV8 for liver targeting, several exhibited a liver detargeting phenotype. Among these, we focused on the N271D variant (AAV8 VP1 numbering), located in the variable region I (VR-1), which has been previously implicated in influencing liver tropism (Cabanes-Creus M et al. *Molecular Therapy Methods & Clinical Development* 2021; Zinn E et al. *Cell Reports Medicine* 2022). The liver detargeting phenotype of AAV8.N271D was confirmed by single vector administration in mice. Additionally, we grafted the N271D variant onto AAV9 and MyoAAV capsids (N270D by AAV9 VP1 numbering). The AAV9.N270D and MyoAAV.N270D vectors showed a similar liver-detargeting phenotype, although muscle targeting was moderately reduced. This study reinforces the important role of VR-1 in modulating liver tropism, and highlights the potential of engineering the VR-1 residues to mitigate liver gene transfer and associated toxicity.

INTRODUCTION

Adeno-associated virus (AAV) has a single-stranded DNA genome packaged in an icosahedral capsid that consists of 60 protein monomers, VP1, VP2, and VP3[1]. The capsid initiates interactions with the host, including binding to cell surface receptors and recognition by the host immune system. In recombinant AAV (rAAV), which is widely used as an *in vivo* gene therapy delivery platform[2], the capsid is either identical to or derived from wild-type AAV, and therefore is inherently critical to determine therapeutically relevant properties, including tissue tropism and immunogenicity. To develop AAV capsids with clinically favorable properties, one way is to isolate the capsid sequences that exist in nature followed by testing in the context of rAAV. This approach has led to the discovery of a series of AAV capsid serotypes[3], many of which have been used in clinical gene therapy and continue to serve as the workhorse for approved AAV-based gene therapies to date[4]. Additionally, these naturally occurring AAV capsid variants provide the foundation for capsid engineering by diverse methods to further improve desired rAAV attributes[5].

From a biology perspective, these naturally occurring AAV capsid sequences offer ample opportunities to study the sequence- and structure-function relationship. For example, aligning the amino acid sequences of various AAV capsids results in the identification of nine variable regions (VRs), which diverge to a higher degree than the remaining regions among different serotypes. Structural studies revealed that VR-I to VR-IX are exposed to the outer surface of the assembled capsid, and play critical roles in binding to a diverse array of cell surface receptors and host antibodies[6]. Understanding the capsid-host interactions at the molecular level allows rational engineering by manipulating specific residues to achieve desired capsid properties[7,8]. Recent high-throughput, long-read DNA sequencing technologies have enabled more efficient and in-depth profiling of naturally existing AAV capsid variants. For example, we previously identified more than 1,000 unique AAV capsid variants from human clinical biopsies using the PacBio sequencing platform[9]. An AAV2-

derived variant, named AAVv66, exhibits enhanced production yields, virion stability, and central nervous system (CNS) transduction[9].

Two liver-targeted gene therapies delivered by AAV vectors have been approved for treating hemophilias A and B, respectively. In both cases, therapeutic levels of the blood clotting factor VIII[10] or factor IX[11] secreted from the liver into the bloodstream could be attained. However, transducing the liver to function as a bio-factory for producing and secreting alpha-1 antitrypsin, the second most abundant secreted serum protein[12], proved challenging in reaching the therapeutic threshold in the bloodstream[13], suggesting that more efficient liver targeting may be required. In our previous capsid discovery study[9], a large portion of the identified capsid variants are AAV8-derived (i.e., exhibiting the highest degree of sequence homology to AAV8). Given AAV8's strong liver tropism, in this study, we tapped into this diverse repertoire of AAV8 variants to characterize their liver tropism in mice and ferrets using a barcoded library screen approach. Although found that no variants surpassed AAV8 for liver gene transfer, we identified one variant with a liver detargeting phenotype mediated by a single N271D residue change in VR-1 (AAV8 VP1 numbering). This study adds to the recent literature showing the important role of VR-1 in liver gene transfer[14,15]. Furthermore, several studies on systemic AAV vector administration have demonstrated liver toxicity[16-19], suggesting the potential safety benefit with a liver-detargeting capsid to deliver gene therapy to other organs, such as the CNS and muscle. The key VR-1 residues that influence liver gene transfer identified by us and others may provide a rational avenue to develop AAV vectors with reduced liver toxicity.

RESULTS

Generation and characterization of an AAV8 vector library

We first constructed a total of 159 packaging plasmids, each expressing a unique AAV8 capsid variant identified from human tissues along with the AAV2 Rep. These plasmids were used individually

to package an *EGFP* transgene cassette in a small-scale AAV vector production assay to determine their vector production yield and to benchmark against the parental AAV8 capsid. Overall, the AAV8 capsid variants were less efficient than AAV8, exhibiting 63% or lower vector production yield **(Figure 1a)**. We arbitrarily selected the top 30% for the subsequent library screen, as low vector production yield will pose a translational hurdle for a gene therapy delivery vehicle.

Next, we constructed a series of gene-of-interest (GOI) plasmids, each expressing a barcoded, non-coding Tough Decoy (TuD) RNA under the control of the U6 promoter as previously reported[20]. We chose not to use a protein-coding reporter transgene, such as *EGFP,* to avoid potential immunogenicity when conducting the screen in large animals such as ferrets. A pair of unique packaging and GOI plasmids were used in large-scale AAV vector production, so that each barcoded *TuD* transgene represented a unique capsid. These vectors were individually purified, followed by vector genome (vg) titer determination. According to their vg titers, these vectors were then pooled at various volumes with the goal of equal representation for each capsid vector in the library. We extracted the pooled library vector DNA, amplified the region with barcodes by PCR, and conducted high-throughput nanopore sequencing to quantify the relative abundance of each barcode, which in turn reflected the relative abundance of each capsid vector in the library. We found that the abundance of the 39 capsid vectors (i.e., AAV8, AAV9, and the 37 AAV8 variants) deviated from the average by less than 2.5-fold **(Figure 1b)**, comparable to other barcoded libraries generated in the same manner (approximately 7-fold)[21]. In contrast, purifying all capsid vectors in bulk would likely result in skewed representation in favor of "good producers" (e.g., more than 200-fold deviation from the average[21]), which may cause bias in subsequent functional screens.

Vector library screen in mice and ferrets

The pooled vector library was delivered to three adult wild-type (WT) mice at 2×10^{13} vg/kg via tail vein. Four weeks post-treatment, the mice were euthanized for tissue collection. The total DNA extracted from livers was subjected to PCR to amplify the vector DNA region with barcodes. The barcodes present in the amplicons were quantified by next-generation sequencing (NGS) and normalized to their relative abundance in the vector library. This analysis revealed that no candidate variants could surpass AAV8 for liver gene delivery **(Figure 2a)**. In parallel, the same vector library was screened in three WT ferrets in the same fashion, which led to the similar finding that AAV8 outperformed all candidate variants **(Figure 2b)**. Notably, the candidate variants generally exhibited a similar trend of liver gene delivery efficiency in mice and ferrets **(Figure 2c)**, suggesting the robustness of the screening pipeline. As several studies have shown that low AAV vector DNA abundance in tissues does not necessarily result in low functional transduction (i.e., transgene expression level)[22-24], we also quantified the barcoded *TuD* RNA levels in mouse livers. However, consistent with the vector DNA analysis, AAV8 outperformed all variants in terms of transgene expression **(Figure 3a**, blue bars**)**.

Liver detargeting by several capsid variants

In both mice and ferrets, we consistently observed that several capsid variants, including v2, v5, v12, v13, v15, v23, v25, and v36, showed very low or barely detectable levels of liver gene delivery **(Figure 2a, b)**. As expected, these candidate variants also led to low or barely detectable *TuD* RNA levels in the mouse livers **(Figure 3a)**. To investigate whether these capsid variants lost liver-specific or pan-tissue tropism, we quantified the *TuD* RNA levels in the heart and tibialis anterior (TA) muscle from the treated mice. Taken together, the RNA analysis revealed that several variants, including v2, v5, v23, v25, and v36, showed a strong liver detargeting phenotype, albeit with moderate reductions in *TuD* expression in the heart and TA muscle. In contrast, transduction by v12, v13, and v15 failed in all three tissue types **(Figure 3a)**.

The N271D (AAV8 VP1 numbering) residue change in v5 is located in VR-1, which had been implicated in modulating liver tropism in recent publications[14,15] **(Figure 3b)** (also see Discussion). Therefore, we focused on this variant for further validation by single vector treatment.

Validation of liver detargeting in mice by single vector administration

To further characterize the impact of N271D on tissue tropism in mice, we generated a pair of AAV8 and AAV8.N271D vectors packaging the same *EGFP* transgene cassette, and treated two groups of mice with the two vectors, respectively. Four weeks post-treatment, the mice were euthanized to compare vector DNA abundance, *EGFP* mRNA levels, and EGFP protein levels in the liver, heart, and TA muscle. Consistent with the library screen results, the AAV8.N271D.EGFP vector showed >100-fold reductions in vector DNA abundance and transgene expression in the liver as compared to the AAV8.EGFP vector, while heart and TA muscle targeting was moderately impacted **(Figure 4a, Supplementary Figure 1)**.

As N271 (AAV8 VP1 numbering) is highly conserved among multiple serotypes **(Figure 3b)**, we tested whether grafting the N271D residue change to other AAV capsids could confer liver detargeting. To this end, we introduced the homologous N270D (AAV9 VP1 numbering) mutation into the AAV9 capsid and generated the AAV9.N270D.EGFP vector. Following administration to WT mice, we observed a dramatic liver detargeting phenotype as compared to the parental AAV9.EGFP vector **(Figure 4b)**. Regarding transducing the heart and TA muscle, N270D in AAV9 capsid had a larger negative impact than N271D in AAV8 (compare the middle panels in **Figures 4a and 4b**). MyoAAV is an engineered capsid with a 7-mer peptide insertion in AAV9, and exhibits enhanced muscle tropism as compared with AAV9 in mice and monkeys[25]. We tested a pair of MyoAAV.EGFP and MyoAAV.N270D.EGFP vectors and again observed liver detargeting in mice **(Figure 4c)**. Although MyoAAV.N270D.EGFP led to lower transduction levels in the heart and TA muscle as compared to

MyoAAV.EGFP, it still outperformed AAV9.EGFP and AAV8.EGFP (compare the middles panels of **Figures 4a-c**).

DISCUSSION

Residues in VR-1 have been shown to influence liver tropism of AAV vectors. Using a domain swapping strategy, Cabanes-Creus et al. found that a single threonine insertion downstream of residue 264 of AAV3B (AAV3B-265*insT*, **Figure 3b**) greatly enhanced liver targeting in mouse[14]. In another study, Zinn et al. identified residue 267 (AAV9 VP1 numbering), named “liver toggle”, as a key determinant for liver targeting[15] **(Figure 3b)**. For example, a single G267A mutation in the AAV9 capsid (AAV9-GA) resulted in significant liver detargeting with respect to both vector genomes (1,522-fold) and expression (363-fold), with no significant difference in terms of gene transfer to the heart and quadriceps, and a moderate reduction in expression in these tissues (1.5-fold and 3.1-fold reductions in quadriceps and heart RNA, respectively)[15]. The N271D (AAV8 VP1 numbering) variant identified in this study is in VR-1 and in proximity with the previously described residues **(Figure 3b)**, and also shows a profound impact on liver targeting. Together, these converging evidence points to the important role of VR-1 in determining liver targeting. Although the detailed mechanism remains to be elucidated, it may involve interactions with AAVR[26], a cellular factor that binds to most AAV capsids and facilitates their cell entry and intracellular trafficking, as structural studies have shown that VR-1 is part of the AAVR-AAV binding footprint[27,28].

The dramatic liver detargeting phenotype of the AAV8.N271D, AAV9.N270D, and MyoAAV.N270D vectors is accompanied by moderate reductions in targeting the heart and TA muscle **(Figure 4)**. A similar trend (i.e., profound liver detargeting with a moderate impact on heart and quadriceps targeting) was also observed when reprogramming AAV9 and Anc80 with the liver toggle residue changes[15]. This creates a dilemma in developing liver-detargeting vectors for gene therapy

delivery to muscle tissues. However, the MyoAAV.N270D vector partially retains the excellent muscle targeting property of the parental MyoAAV capsid, and exhibits higher gene transfer and expression levels in the heart and TA muscle than the AAV8 and AAV9 vectors. Furthermore, it may be possible to engineer the residues in VR-1 or in combination with other capsid regions to develop true liver-specific detargeting capsids.

In summary, this study identifies a naturally occurring AAV capsid variant that shows a liver detargeting phenotype. It reinforces the notion that VR-1 plays an important role in modulating liver tropism and expression, and provides new avenues to engineer AAV vectors that spare liver targeting and reduce liver toxicity.

MATERIALS AND METHODS

AAV constructs

The reporter transgene construct used in the small-scale AAV vector production assay contains an *EGFP* transgene under the control of the CMV enhancer and chicken beta-actin promoter. The same construct was packaged in multiple capsids for single vector administration in mice. The barcoded transgene construct used for generating AAV vector library contains a *TuD* transgene under the control of the U6 promoter. The detailed design of barcode has been described previously[20]. Briefly, the barcode contains randomized 8 nucleotides that are embedded in the microRNA binding site (MBS) between stem I and stem II of the *TuD* transgene DNA, and it is also present in the *TuD* RNA following expression. All AAV constructs were designed to package single-stranded vector genomes.

Small-scale AAV vector production assay

The details of the procedure have been described previously[29]. Briefly, a pair of packaging plasmid and gene-of-interest (GOI) plasmid were transfected to HEK293 cells along with a helper

plasmid in a 12-well plate using the CsCl method. 48 hours post-transfection, cells and culture media were collected to generate crude lysates following three freeze-and-thaw cycles. The crude lysates were clarified by centrifugation and sequentially treated with DNase I and proteinase K, followed by vector genome determination using droplet digital PCR (ddPCR).

Nanopore sequencing of amplicons

AAV vector DNA was extracted with the QIAamp DNA Micro Kit (Qiagen, 56304), and subjected to PCR amplification. The amplicons were purified with the DNA Clean & Concentrator-5 kit (Zymo, D4013) and sequenced with the Oxford Nanopore platform (Plasmidsaurus). Reads were mapped to the reference sequence, demultiplexed by barcodes, and counted using the Geneious Prime software.

Large-scale AAV vector production

Adherent HEK293 cells were cultured in roller bottles in Dulbecco's Modified Eagle Medium (DMEM) with 10% fetal bovine serum. Helper plasmid, packaging plasmid, and GOI plasmid were co-transfected using the calcium chloride method. Next day, the cell culture medium was replaced with fresh, serum-free DMEM. Three days post-transfection, cells and culture media were harvested and subjected to purification using two rounds of cesium chloride gradient centrifugation. AAV vectors were dialyzed against phosphate buffered saline and sterilized by passing through a 0.22 μm filter.

Animal work

Wildtype, male C57BL/6J mice were treated with AAV vectors via tail vein at six weeks of age, and euthanized four weeks later. For library screen, the dose was 5×10^{11} vg/mouse (approximately 2×10^{13} vg/kg); for single vector administration, the dose was 3×10^{11} vg/mouse. Three wildtype ferrets at 10 weeks of age (one female and two males) were treated with the AAV vector library via intravenous injection at the dose of 2×10^{13} vg/kg, and euthanized five weeks later. All animal studies were reviewed and approved by the Institutional Animal Care and Use Committee of the University of Massachusetts Chan Medical School.

Quantification of barcodes by next-generation sequencing

DNA and RNA were isolated from liver samples using the AllPrep DNA/RNA kit (Qiagen, 80204). For muscle tissues, DNA was extracted with the AllPrep DNA/RNA kit (Qiagen, 80204), while RNA was extracted using Trizol. RNA was subjected to treatment with DNase (Qiagen 79254) followed by a clean-up step using the RNA Clean & Concentrator-5 kit (Zymo, R1014). Purified RNA was reverse-transcribed into cDNA using the SuperScript III First-Strand Synthesis System (Thermo Fisher Scientific, 18080051). PCR was performed with barcoded primers and the KAPA HiFi HotStart ReadyMix (Roche, KK2602). PCR amplicons were gel purified and concentrations were determined using a Qubit 3 Fluorometer (Thermo Fisher Scientific). PCR amplicons were pooled at an equal ratio and sequenced using Illumina HiSeq at UMass Chan Deep Sequencing Core. Sequencing data were analyzed using the Galaxy platform[30].

Quantification of vector DNA and RNA

DNA and RNA were isolated from mouse tissues using the AllPrep DNA/RNA kit (Qiagen, 80204). RNA was reverse-transcribed into cDNA with the High-Capacity cDNA Reverse Transcription kit (Thermo Fisher Scientific, 43-688-13). To quantify vector DNA, a duplexing Taqman droplet digital PCR (ddPCR) assay was performed with one reagent targeting *EGFP* (Thermo Fisher Scientific, Mr00660654_cn), and the other targeting *Tfrc* (Thermo Fisher Scientific, 4458367). cDNA was quantified using a duplexing Taqman ddPCR assay with the same *EGFP*-targeting Taqman reagent as mentioned above, and a Taqman reagent targeting *Gapdh* (Thermo Fisher Scientific, 4352339E). ddPCR was performed with a QX200 instrument (Bio-Rad).

Western blot

Mouse tissues were homogenized using TissueLyser II (Qiagen) in ice-cold T-PER (Thermo Fisher Scientific, 78510) with protease inhibitor (Roche, 4693159001). Total protein concentration in tissue lysate was determined with Pierce BCA Protein Assay Kit (Pierce,

23225). Protein lysates normalized for total protein amount were boiled with 4× Laemmli sample buffer (Bio-Rad, 1610747) at 99 °C for 5 min. Primary antibodies: mouse anti-EGFP Antibody (Abcam, ab184601, 1:5000), rabbit anti-GAPDH (Abcam, ab9485, 1:10000). Secondary antibodies: LICOR IRDye 680RD goat anti-mouse IgG (H + L) (LI-COR Biosciences, 926-68070, 1:7000), LICOR IRDye 800CW goat anti-rabbit IgG (H + L) (LI-COR Biosciences, 926-32211, 1:7000). Blot membranes were imaged by LI-COR scanner (Odyssey) and quantified by Li-Cor software.

ACKNOWLEDGEMENTS

This study was supported by a grant from the National Institutes of Health (NIH) (P01HL158506 to D.W.). The Gao Lab is supported by grants from the NIH (R01NS076991-01, P01AI100263-01, P01HL131471-02, 35 R01AI121135, UG3HL147367-01, R01HL097088, and U19AI149646-01) and Cystic Fibrosis Foundation.

AUTHOR CONTRIBUTIONS

R.X., D.W. designed the research. R.X., M.X. conducted the majority of the experiments. D.R., A.D., A.M.G. performed injections in ferrets and other ferret work. R.X., M.C., P.W.L.T. contributed to NGS data analysis. G.X., L.L., M.X., F.Z., P.W.L.T., G.G. provided the AAV8 variants. N.L. produced AAV vectors. J.L. performed mouse injections and other mouse work. T.R.F., G.G., D.W. supervised the study. R.X., M.X., D.W. analyzed data and wrote the manuscript.

DECLARATION OF INTERESTS

G.G. is a scientific co-founder of Voyager Therapeutics, Adrenas Therapeutics and Aspa Therapeutics and holds equity in these companies.

KEYWORDS

AAV, liver detargeting, liver tropism, variable region

REFERNCES

1. Muzyczka, N., and Berns, K. (2001). Parvoviridae: the viruses and their replication. In Fields Virology, D. Knipe, P. Howley, D. Griffin, R. Lamb, M. Martin, B. Roizman, and S. Straus, eds. (Philadelphia, PA: Lippincott, Williams and Wilkins), pp. 2327-2359.
2. Wang, D., Tai, P.W.L., and Gao, G. (2019). Adeno-associated virus vector as a platform for gene therapy delivery. *Nat Rev Drug Discov* 18, 358-378.
3. Gao, G., Vandenberghe, L.H., Alvira, M.R., Lu, Y., Calcedo, R., Zhou, X., and Wilson, J.M. (2004). Clades of Adeno-associated viruses are widely disseminated in human tissues. *J Virol* 78, 6381-6388.
4. ASGCT (2025). Gene, Cell, & RNA Therapy Landscape Report (Q4 2024 Quarterly Data Report). https://www.asgct.org/global/documents/asgct-citeline-q4-2024-report.aspx.
5. Li, C., and Samulski, R.J. (2020). Engineering adeno-associated virus vectors for gene therapy. *Nat Rev Genet* 21, 255-272.
6. Agbandje-McKenna, M., and Kleinschmidt, J. (2011). AAV capsid structure and cell interactions. *Methods Mol Biol* 807, 47-92.
7. Asokan, A., Conway, J.C., Phillips, J.L., Li, C., Hegge, J., Sinnott, R., Yadav, S., DiPrimio, N., Nam, H.J., Agbandje-McKenna, M., McPhee, S., Wolff, J., and Samulski, R.J. (2010). Reengineering a receptor footprint of adeno-associated virus enables selective and systemic gene transfer to muscle. *Nat Biotechnol* 28, 79-82.
8. Tseng, Y.S., and Agbandje-McKenna, M. (2014). Mapping the AAV Capsid Host Antibody Response toward the Development of Second Generation Gene Delivery Vectors. *Front Immunol* 5, 9.
9. Hsu, H.L., Brown, A., Loveland, A.B., Lotun, A., Xu, M., Luo, L., Xu, G., Li, J., Ren, L., Su, Q., Gessler, D.J., Wei, Y., Tai, P.W.L., Korostelev, A.A., and Gao, G. (2020). Structural characterization of a novel human adeno-associated virus capsid with neurotropic properties. *Nat Commun* 11, 3279.
10. Mahlangu, J., Kaczmarek, R., von Drygalski, A., Shapiro, S., Chou, S.C., Ozelo, M.C., Kenet, G., Peyvandi, F., Wang, M., Madan, B., Key, N.S., Laffan, M., Dunn, A.L., Mason, J., Quon, D.V., et al. (2023). Two-Year Outcomes of Valoctocogene Roxaparvovec Therapy for Hemophilia A. *N Engl J Med* 388, 694-705.

11. Pipe, S.W., Leebeek, F.W.G., Recht, M., Key, N.S., Castaman, G., Miesbach, W., Lattimore, S., Peerlinck, K., Van der Valk, P., Coppens, M., Kampmann, P., Meijer, K., O'Connell, N., Pasi, K.J., Hart, D.P., et al. (2023). Gene Therapy with Etranacogene Dezaparvovec for Hemophilia B. *N Engl J Med* 388, 706-718.

12. Strnad, P., McElvaney, N.G., and Lomas, D.A. (2020). Alpha(1)-Antitrypsin Deficiency. *N Engl J Med* 382, 1443-1455.

13. Blackwood, M., Gruntman, A.M., Tang, Q., Pires-Ferreira, D., Reil, D., Kondratov, O., Marsic, D., Zolotukhin, S., Gernoux, G., Keeler, A.M., Mueller, C., and Flotte, T.R. (2024). Biodistribution and safety of a single rAAV3B-AAT vector for silencing and replacement of alpha-1 antitrypsin in Cynomolgus macaques. *Mol Ther Methods Clin Dev* 32, 101200.

14. Cabanes-Creus, M., Navarro, R.G., Liao, S.H.Y., Baltazar, G., Drouyer, M., Zhu, E., Scott, S., Luong, C., Wilson, L.O.W., Alexander, I.E., and Lisowski, L. (2021). Single amino acid insertion allows functional transduction of murine hepatocytes with human liver tropic AAV capsids. *Mol Ther Methods Clin Dev* 21, 607-620.

15. Zinn, E., Unzu, C., Schmit, P.F., Turunen, H.T., Zabaleta, N., Sanmiguel, J., Fieldsend, A., Bhatt, U., Diop, C., Merkel, E., Gurrala, R., Peacker, B., Rios, C., Messemer, K., Santos, J., et al. (2022). Ancestral library identifies conserved reprogrammable liver motif on AAV capsid. *Cell Rep Med* 3, 100803.

16. Chand, D., Mohr, F., McMillan, H., Tukov, F.F., Montgomery, K., Kleyn, A., Sun, R., Tauscher-Wisniewski, S., Kaufmann, P., and Kullak-Ublick, G. (2021). Hepatotoxicity following administration of onasemnogene abeparvovec (AVXS-101) for the treatment of spinal muscular atrophy. *J Hepatol* 74, 560-566.

17. Hudry, E., Aihara, F., Meseck, E., Mansfield, K., McElroy, C., Chand, D., Tukov, F.F., and Penraat, K. (2023). Liver injury in cynomolgus monkeys following intravenous and intrathecal scAAV9 gene therapy delivery. *Mol Ther* 31, 2999-3014.

18. Hordeaux, J., Lamontagne, R.J., Song, C., Buchlis, G., Dyer, C., Buza, E.L., Ramezani, A., Wielechowski, E., Greig, J.A., Chichester, J.A., Bell, P., and Wilson, J.M. (2024). High-dose systemic adeno-associated virus vector administration causes liver and sinusoidal endothelial cell injury. *Mol Ther* 32, 952-968.

19. Whiteley, L.O. (2023). An Overview of Nonclinical and Clinical Liver Toxicity Associated With AAV Gene Therapy. *Toxicol Pathol* 51, 400-404.

20. Xu, M., Li, J., Xie, J., He, R., Su, Q., Gao, G., and Tai, P.W.L. (2019). High-Throughput Quantification of In Vivo Adeno-Associated Virus Transduction with Barcoded Non-Coding RNAs. *Hum Gene Ther* 30, 946-956.

21. Weinmann, J., Weis, S., Sippel, J., Tulalamba, W., Remes, A., El Andari, J., Herrmann, A.K., Pham, Q.H., Borowski, C., Hille, S., Schonberger, T., Frey, N., Lenter, M., VandenDriessche, T., Muller, O.J., et al. (2020). Identification of a myotropic AAV by massively parallel in vivo evaluation of barcoded capsid variants. *Nat Commun* 11, 5432.

22. Salganik, M., Aydemir, F., Nam, H.J., McKenna, R., Agbandje-McKenna, M., and Muzyczka, N. (2014). Adeno-associated virus capsid proteins may play a role in transcription and second-strand synthesis of recombinant genomes. *J Virol* 88, 1071-1079.

23. Gonzalez-Sandoval, A., Pekrun, K., Tsuji, S., Zhang, F., Hung, K.L., Chang, H.Y., and Kay, M.A. (2023). The AAV capsid can influence the epigenetic marking of rAAV delivered episomal genomes in a species dependent manner. *Nat Commun* 14, 2448.

24. Loeb, E.J., Havlik, P.L., Elmore, Z.C., Rosales, A., Fergione, S.M., Gonzalez, T.J., Smith, T.J., Benkert, A.R., Fiflis, D.N., and Asokan, A. (2024). Capsid-mediated control of adeno-associated viral transcription determines host range. *Cell Rep* 43, 113902.

25. Tabebordbar, M., Lagerborg, K.A., Stanton, A., King, E.M., Ye, S., Tellez, L., Krunnfusz, A., Tavakoli, S., Widrick, J.J., Messemer, K.A., Troiano, E.C., Moghadaszadeh, B., Peacker, B.L., Leacock, K.A., Horwitz, N., et al. (2021). Directed evolution of a family of AAV capsid variants enabling potent muscle-directed gene delivery across species. *Cell* 184, 4919-4938 e4922.

26. Pillay, S., Meyer, N.L., Puschnik, A.S., Davulcu, O., Diep, J., Ishikawa, Y., Jae, L.T., Wosen, J.E., Nagamine, C.M., Chapman, M.S., and Carette, J.E. (2016). An essential receptor for adeno-associated virus infection. *Nature* 530, 108-112.

27. Zhang, R., Cao, L., Cui, M., Sun, Z., Hu, M., Zhang, R., Stuart, W., Zhao, X., Yang, Z., Li, X., Sun, Y., Li, S., Ding, W., Lou, Z., and Rao, Z. (2019). Adeno-associated virus 2 bound to its cellular receptor AAVR. *Nat Microbiol* 4, 675-682.

28. Meyer, N.L., Hu, G., Davulcu, O., Xie, Q., Noble, A.J., Yoshioka, C., Gingerich, D.S., Trzynka, A., David, L., Stagg, S.M., and Chapman, M.S. (2019). Structure of the gene therapy vector, adeno-associated virus with its cell receptor, AAVR. *Elife* 8.

29. Ai, J., Ibraheim, R., Tai, P.W.L., and Gao, G. (2017). A Scalable and Accurate Method for Quantifying Vector Genomes of Recombinant Adeno-Associated Viruses in Crude Lysate. *Hum Gene Ther Methods* 28, 139-147.

30. Galaxy, C. (2024). The Galaxy platform for accessible, reproducible, and collaborative data analyses: 2024 update. *Nucleic Acids Res* 52, W83-W94.

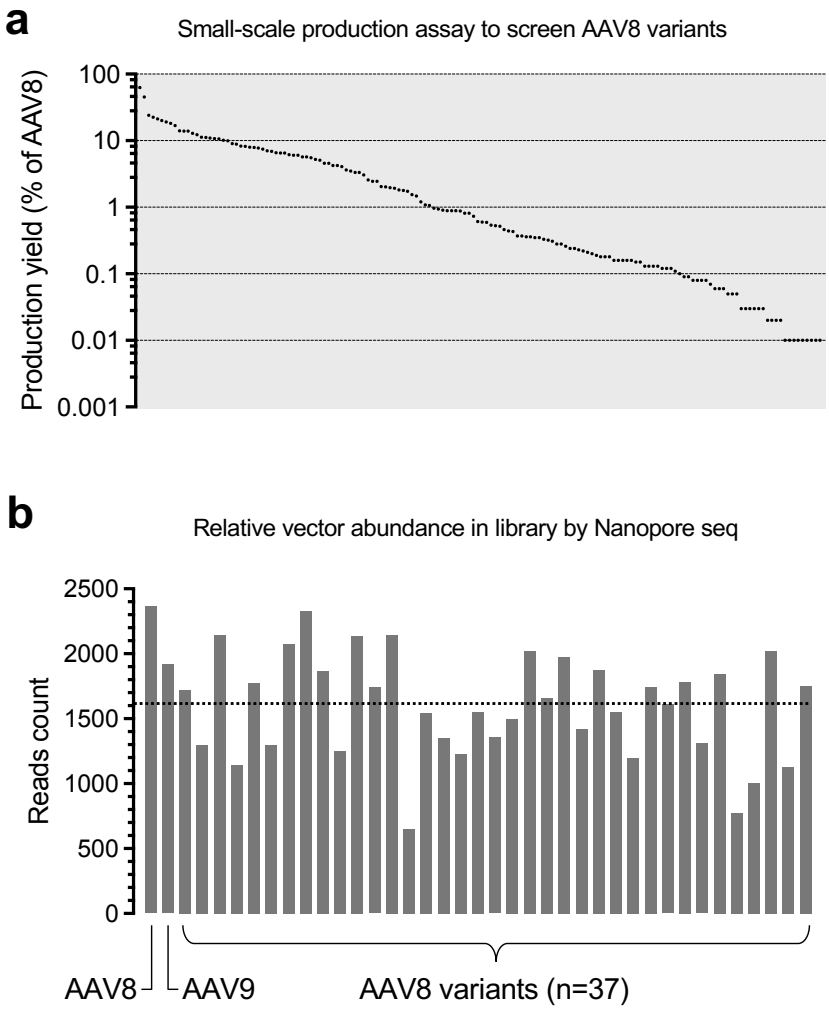

Figure 1. Generation and characterization of AAV8 vector library. (a) Dot plot showing the production yield of each AAV8 capsid variant in a small-scale vector production assay packaging the same *EGFP* transgene cassette. Each dot represents a unique capsid variant. The production yield is normalized to the AAV8 vector level (defined as 100%) and ranked from the highest to the lowest. **(b)** Bar graph showing the count of Nanopore sequencing reads mapped to the unique vector transgene barcodes packaged in AAV8, AAV9, or AAV8 variants. The dashed line shows the mean value.

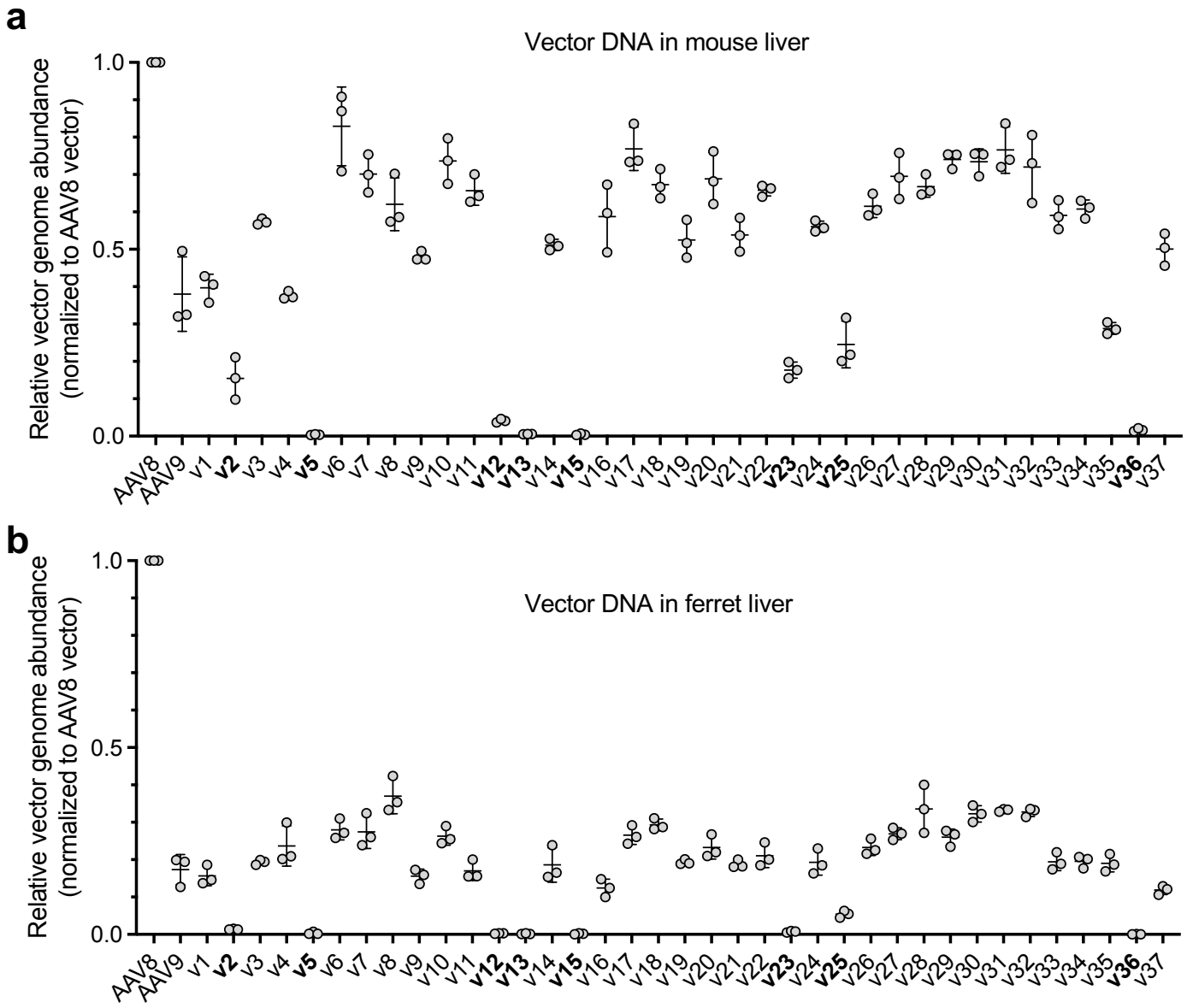

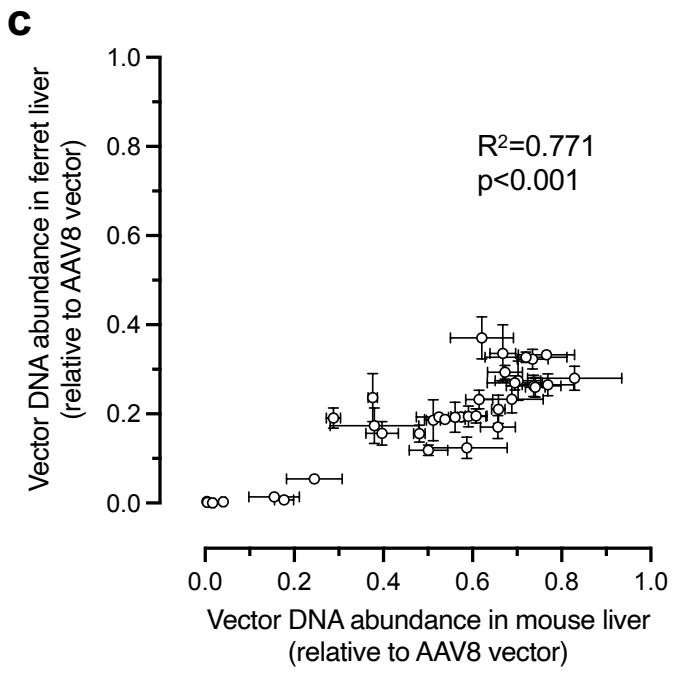

Figure 2. Vector library screen in mice and ferrets. (a, b) Scatter dot plots showing the relative vector genome abundance of each barcoded capsid vector in mouse (a) or ferret (b) livers. Data are normalized to the AAV8 vector level (defined as 1.0), and presented as mean ± SD. Each dot represents an individual animal. v1 to v37 denote the identifiers of AAV8 variants. The variants in bold indicate that they resulted in low or barely detectable levels of vector DNA. **(c)** Scatter plot showing the relationship between the relative vector DNA abundance of each capsid variant in mouse liver (x-axis) and ferret liver (y-axis). Data are presented as mean and standard deviation of three animals. The linear regression statistics are shown.

a

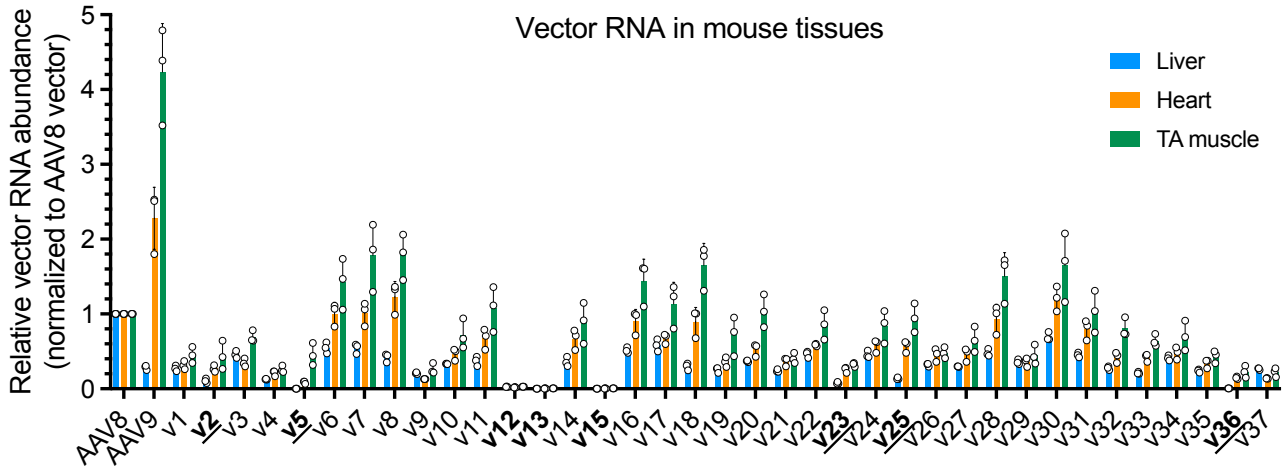

b

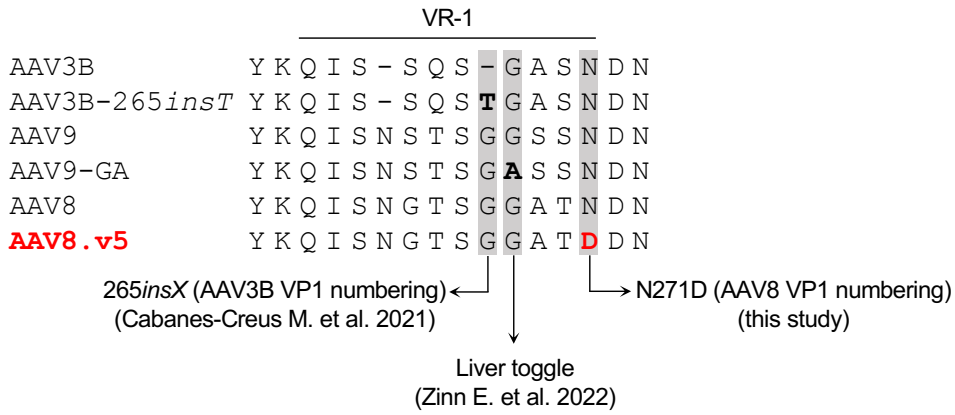

Figure 3. AAV8.v5 shows liver detargeting phenotype in mice. (a) Bar graph showing the relative vector RNA (cDNA) abundance of each barcoded capsid vector in mouse liver (blue), heart (orange), and tibialis anterior (TA) muscle (green). Data are normalized to the AAV8 vector level in respective tissues (defined as 1), and presented as mean ± SD. Each dot represents an individual animal. v1 to v37 denote the identifiers of AAV8 variants. The variants in bold indicate that they resulted in low or barely detectable levels of vector RNA expression in the liver, with the ones underlined indicating well-detectable levels of vector RNA expression in the heart and/or TA muscle. **(b)** Alignment of the amino acid sequences of multiple AAV capsids. Only variable region I (VR-1) and surrounding residues are shown as single-letter abbreviations. Dashes indicate gaps. The 265*insT* (AAV3B VP1 numbering) residue described in Cabanes-Creus M. et al. 2021, the liver toggle residue described in Zinn E. et al. 2022, and the N271D (AAV8 VP1 numbering) residue described in this study are highlighted with gray background. The residues that differ from parental capsids described in these studies are highlighted in bold.

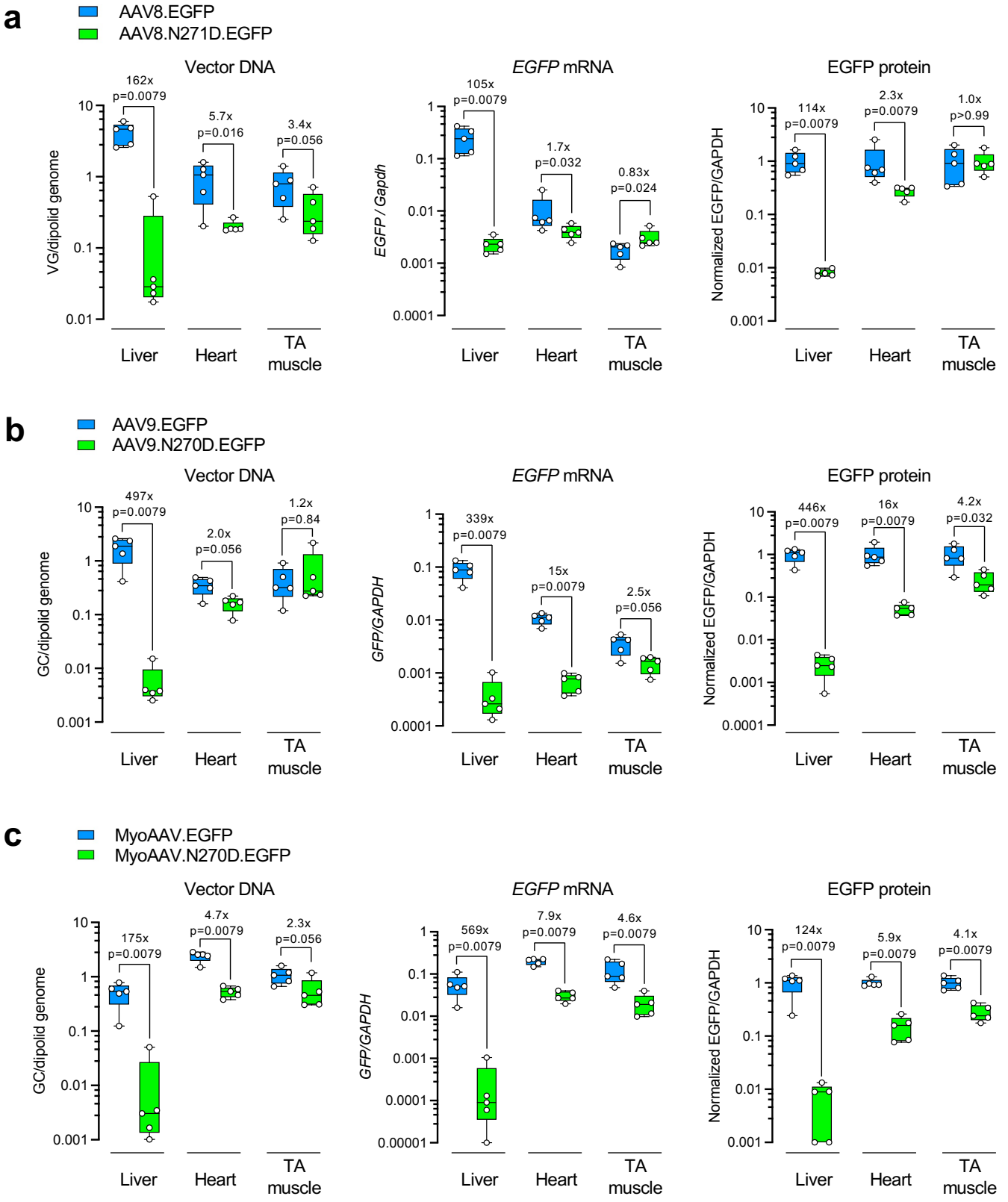

Figure 4. Characterization of vector performance in mice following individual vector administration. (a-c) Box plots showing the vector DNA abundance (left), *EGFP* mRNA levels (middle), and EGFP protein levels (right) in the liver, heart, and tibialis anterior (TA) muscle collected from the mice treated with AAV8 or AAV8.N271D vectors (a), AAV9 or AAV9.N270D vectors (b), and MyoAAV or MyoAAV.N270D vectors (c). Each dot represents an individual mouse. The box extends from the first to the third quartiles with the line inside denoting median. The whiskers end at minimum and maximum values. The fold changes of medians and p values are labeled. Statistical analysis is performed using non-parametric Mann-Whitney test.